Modification of Loop 1 Affects the Nucleotide-Binding Properties of Myo1c, The Adaptation Motor in the Inner Ear[†]

Nancy Adamek,
University of Kent, Canterbury, Kent, CT2 7NJ, U.K.

Alena Lieto-Trivedi,
Boston Biomedical Research Institute, Watertown, MA 02472, U.S.A.

Michael A. Geeves, and
University of Kent, Canterbury, Kent, CT2 7NJ, U.K.

Lynne M. Coluccio[*]
Boston Biomedical Research Institute, Watertown, MA 02472, U.S.A.

Abstract

Myo1c is one of eight members of the mammalian myosin I family of actin-associated molecular motors. In stereocilia of the hair cells in the inner ear, Myo1c presumably serves as the adaptation motor, which regulates the opening and closing of transduction channels. Although there is conservation of sequence and structure among all myosins in the N-terminal motor domain, which contains the nucleotide- and actin-binding sites, some differences include the length and composition of surface loops, including loop 1, which lies near the nucleotide-binding domain. To investigate the role of loop 1, we expressed in insect cells mutants of a truncated form of Myo1c, Myo1c^{1IQ}, as well as chimeras of Myo1c^{1IQ} with the analogous loop from other myosins. We found that replacement of the charged residues in loop 1 with alanines or the whole loop with a series of alanines did not alter the ATPase activity, transient kinetics properties and Ca^{2+}-sensitivity of Myo1c^{1IQ}. Substitution of loop 1 with that of the corresponding region from tonic smooth muscle myosin II (Myo1c^{1IQ}-tonic) or replacement with a single glycine (Myo1c^{1IQ}-G) accelerated ADP release from A.M 2-3-fold in Ca^{2+}, whereas substitution with loop 1 from phasic muscle myosin II (Myo1c^{1IQ}-phasic) accelerated ADP release 35-fold. Motility assays with chimeras containing a single α-helix, or SAH, domain showed that Myo1c^{SAH}-tonic translocated actin in vitro twice as fast as Myo1c^{SAH}-WT and 3-fold faster than Myo1c^{SAH}-G. The studies show that changes induced in Myo1c by modifying loop 1 showed no resemblance to the behaviour of the loop donor myosins or to the changes previously observed with similar Myo1b chimeras.

Myosins are a large family of molecular motors that have been subdivided into more than 30 subgroups (1,2). Different family members are involved in a wide range of motor activities in eukaryotic cells such as muscle contraction, cell division, pseudopod extension and vesicle transport (3,4). Class I myosins are a diverse group of monomeric myosins implicated in several actin-mediated processes including organization and maintenance of tension of the cytoskeleton as well as signal transduction (5-7). The mammalian class I myosin, Myo1c, consists of a heavy chain containing an N-terminal motor domain, a neck or lever arm stabilised by 3 calmodulin molecules and a C-terminal tail region implicated in membrane binding (8-10). Myo1c mediates the cycling of GLUT4 transporters in adipocytes by promoting the

[*]To whom correspondence should be addressed: Boston Biomedical Research Institute, 64 Grove Street, Watertown, MA 02472. Telephone: (617) 658-7784. Fax. (617) 972-1761. coluccio@bbri.org.

fusion of GLUT4-containing vesicles with the cell membrane (11-13). In the specialized hair cells of the inner ear, Myo1c is believed to be the adaptation motor, which regulates the tension on the tip links that connect neighbouring stereocilia thereby controlling the opening and closing of transduction channels (5).

We recently defined the biochemical kinetics of the ATP-driven interaction of Myo1c with actin and showed that it has an unusual calcium dependence (14). Calcium binding to the calmodulin closest to the motor domain has little effect on the ATPase or motor activity, but alters specific steps of the ATPase cycle. ATP hydrolysis was *inhibited* 7-fold by calcium while ADP release from acto-Myo1c was *accelerated* by 10-fold. These two changes together would reduce the lifetime of the actin-*at*tached states and increase the lifetime of the actin-*de*tached state without altering the overall cycle time. In combination these properties appear to be ideal to modulate the activity of Myo1c in response to a calcium transient of the sort expected to occur in the inner ear.

The observation that certain events in the ATPase cycle are regulated oppositely in calcium is curious and in particular the Ca^{2+}-regulation of the ATP hydrolysis step has not been reported previously for any myosin. This raises the question of whether the ATP hydrolysis step is controlled by calcium binding to the calmodulin light chain. In fact, the regulation may occur via the myosin conformational change that precedes the ATP cleavage step and is thought to position the catalytic residues to allow ATP splitting. This conformational change, known as the recovery stroke, involves the movement of switch II and the accompanying converter-domain movement to reprime the lever arm/light-chain domain (15,16). Thus, the recovery stroke results in a repositioning of the light chains and therefore could be influenced by a calcium-induced change in the calmodulin/light chain conformation.

Other events regulated by calcium are ATP binding and ADP release. ADP release in smooth and scallop muscle is altered via phosphorylation or calcium binding to light chains (17,18). The exact mechanism by which the conformation of the light chains is communicated to the nucleotide-binding pocket for these dimeric myosins is not defined, but may involve some form of interaction between the two motor domains facilitated by the conformation of the neck domains (19-21). Although we previously reported a modest regulation of nucleotide release in calcium for the related myosin I, Myo1b, the behaviour of Myo1c is more dramatic (22). The communication pathway of this novel regulation via the light chains for monomeric myosins is unknown.

The structure of the myosin motor domain is highly conserved across the broad myosin family; however, there are several surface loops that are less well conserved. These loops have been proposed to tune the activity of myosins to their specific cellular roles (23). One such loop is loop 1 near the entrance to the nucleotide-binding pocket. Loop 1 joins two helices, one connected to switch 1 and the other to the P-loop. These two elements form a major part of the binding site for the gamma phosphate in ATP. Loop 1 is therefore in a position to influence access to the nucleotide pocket and the interaction with the gamma Pi of ATP. Previous studies of natural variations of loop 1 in vertebrate smooth muscle myosin II (24-26) have shown that alternately expressed loops can alter the release of ADP from the nucleotide pocket. Furthermore, studies on scallop muscle myosin II (27) have established that alternate splicing of loop 1 alters the affinity of acto-myosin for ADP thereby permitting the cell to produce myosins with differing ATPase and motility properties. However, studies of engineered variations in the size and composition of loop 1 in either a smooth muscle myosin II or a *Dictyostelium* myosin II (28) have so far failed to resolve which features of loop 1 are responsible for this modulation of myosin activity.

Goodson and colleagues showed that the sequences of loop 1 are well conserved when myosins are grouped according to their kinetic activity and proposed that loop 1 modulates the kinetic characteristics that distinguish one myosin isoform from another (29). It has also been suggested that the flexibility of loop 1 or its length determines activity (26) and that longer loops interact with other parts of the myosin molecule including the light chains in some conformations thereby affecting regulation (30).

In a previous study (22), we explored the role of loop 1 on Myo1b by replacing its charged residues with alanine, the whole loop with alanine residues or replacing the loop with either a single glycine, or loop 1 from either phasic or tonic smooth muscle myosin II, a strategy similar to that used by others to explore the effects of loop 1 on smooth muscle myosin II (24,26,27). We found that loop 1 had major effects on the coupling of actin and nucleotide-binding events in Myo1b and that it is likely to modulate the load dependence of Myo1b. The role of loop 1 can therefore have broad implications for modulating myosin motor activity; however, the same mutations in different myosin backgrounds can have quite different effects (22,31).

To explore the role of loop 1 in Myo1c we investigated how loop 1 modulates the motor activity of Myo1c, specifically its effects on nucleotide binding and release in the presence and absence of calcium. We found that all the results obtained with the Myo1c chimeras stand in marked contrast to those previously obtained with similar constructs using Myo1b.

Experimental Procedures

Preparation of Constructs and Expression in Insect Cells

Using cDNA encoding the entire open reading frame of Myo1c (previously known as myr 2; the kind gift of Dr. Martin Bähler; Institut für Allgemeine Zoologie und Genetik, Westfälische-Wilhelms Universität, Münster, Germany), we prepared a series of constructs in which loop 1 of Myo1c^{1IQ}, a truncated form of rat Myo1c representing the motor domains and first IQ domain (amino acids 1-725) (32), was replaced with loops 1 from other myosins; or in which alanine substitutions were made in the endogenous loop 1. To define the beginning and end of loop 1 in Myo1c, secondary structure assignments were made by the program DSSP (Definition of Secondary Structure of Protein; http://swift.cmbi.ru.nl/gv/dssp/descrip.html). All mutants except Myo1c^{1IQ}-phasic were created using polymerase chain reaction (PCR). Overlapping sets of primers having the desired mutations and restriction sites and incorporating a FLAG tag at the C-terminus were used in the first set of PCR reactions. The two resulting fragments were then subjected to another round of PCR with the outside primers to generate the in-frame fusion proteins. After treatment with the appropriate restriction enzymes, the purified PCR products were ligated into the pFastBacDUAL transfer vector (Gibco BRL, Gaithersburg, MD) downstream of the polyhedrin promoter; the p10 promoter cloning site contained the gene coding for calmodulin (32). The plasmids were transformed into DH5α cells and selected by antibiotic resistance. Colonies were grown and the isolated DNA was tested for the presence of inserts by restriction analysis. Plasmids containing Myo1c inserts were sequenced with internal and vector-specific oligonucleotides using automated sequencing. Myo1c^{1IQ}-phasic was made using the Transformer Site-Directed Mutagenesis Kit (Clontech, Mountain View, CA 94043). Briefly, a mutagenic primer and a selection primer were used to generate a mixture of mutated and unmutated plasmids. The mixture was then subjected to a selective restriction digestion, which selectively digested the unmutated plasmid. The mutated plasmid was then transformed as above into DH5α followed by selection according to antibiotic resistance. Plasmids were isolated from selected colonies and those containing inserts were subjected to automatic sequencing.

In all cases, the recombinant donor plasmid was transformed into DH10Bac *E. coli* cells (Invitrogen, Carlsbad, Ca 92008) for transposition into bacmid. Recombinant bacmid DNA

was isolated by potassium acetate precipitation as described by the Bac-to-Bac Baculovirus Expression Systems Instruction Manual supplied by Invitrogen. Virus was produced by transfecting the recombinant bacmid DNA into *Spondoptera frugiperda* 9 (Sf9) insect cells with Cellfectin reagent (Invitrogen) followed by 3 days of growth. Subsequently, amplified virus was used to infect Sf9 cells in suspension. Infection was allowed to proceed for 4 days after which time cells were harvested by centrifugation. Cell pellets were either used immediately for protein isolation or frozen in liquid N_2 and stored at -80°C for future use.

Protein purification

To isolate protein, the insect cell pellets were homogenized in 10 mM Tris, pH 7.5, 0.2 M NaCl, 4 mM $MgCl_2$, and 2 mM ATP in the presence of protease inhibitors and then centrifuged at $183,000 \times g$ for 50 min. The supernatant was applied to an anti-FLAG column, and after washing the expressed proteins were eluted with a step gradient of FLAG peptide. Fractions containing protein were identified by SDS-polyacrylamide gel electrophoresis, pooled and dialyzed against 10 mM Tris, 50 mM KCL and 1 mM DTT. Proteins were either used immediately or stored at -80°C for future use.

Preparation of Constructs with a SAH Domain

Using the clone for rat myosin X (kindly provided by Drs. Erich Boger and Thomas Friedman, NIDCD, NIH) we prepared by PCR a fusion construct (Myo1c[SAH]-WT) in which the SAH domain of myosin X (amino acids 805-843) followed by a myc and FLAG tag were added to wild-type Myo1c at residue 762 based on sequence analogy between Myo1c and myosin X as determined by Clustal X. This results in a LCBD consisting of two complete IQ motifs and most of the third IQ motif followed by the SAH domain. The SAH constructs express in insect cells at levels equivalent to the 1IQ forms. Similar constructs for the loop 1 mutants, tonic, phasic and G (Myo1c[SAH]-tonic, Myo1c[SAH]-phasic and Myo1c[SAH]-G, respectively) were also prepared and expressed in insect cells and purified by affinity purification with anti-FLAG.

ATPase Activity

The steady-state actin-activated Mg^{2+}-ATPase activity of Myo1c and the loop 1 mutants (1IQ forms and those incorporating SAH domains) was measured using a colorimetric assay described by Pollard (33) in 10 mM Tris, pH 7.5, 50 mm KCl, 1 mM $MgCl_2$ and $CaCl_2$ and EGTA to effect pCa values ranging from 4 - 8.9.

Motility Assays

The ability of the purified myosins to translocate actin filaments in vitro was determined using a procedure similar to one previously described (34). Briefly, flow chambers were made by attaching nitrocellulose-coated coverslips face down to a glass microscope slide using double-sided sticky tape. Myosin was prepared by mixing it with 0.05 mg/ml F-actin and 10 mM ATP for 20 min, then spinning at $245,00 \times g$ and 4°C for 20 min. The flow chambers were coated with ~12 μl 0.05 mg/ml myc antibody (Invitrogen) in PBS for 15 min, then 75 μl 5 mg/ml bovine serum albumin (BSA) in motility buffer (25 mM Imidazole, pH 7.5, 1 mM EGTA, 25 mM KCL, 4 mM $MgCl_2$) for 10 min to block non-specific sites. Thirty μl myosin supernatant (at various concentrations) was applied to the flow chamber for 15 min then washed with motility buffer plus BSA for 10 min. Thirty μl ~0.14 μM rabbit skeletal muscle F-actin labeled with rhodamine phalloidin (Molecular Probes, Eugene, OR) was applied to the flow chamber for 5 min. The chambers were washed with 75 μl motility buffer plus BSA before adding 50 μl motility buffer containing 0.5% methylcellulose, 3 mg/ml glucose, 20 mM DTT, 0.1 mg/ml glucose oxidase, 0.05 mg/ml catalase and 2 mM ATP. Slides were examined with a fluorescence microscope using a 100× oil immersion lens (Nikon Inc., Melville, NY). Images were recorded digitally using a FlashBus MV PCI bus frame grabber (Integral Technologies,

Inc., Indianapolis, IN). The percentage of translocating filaments was determined using Manually Count Objects, and the speed of the filaments was determined using Track Points in MetaMorph bioimaging software (version 6.3r2, Universal Imaging Corp., Downingtown, PA).

Transient enzyme kinetics

Rapid kinetic measurements were carried out using a standard Hi-Tech Scientific SF-61 DX2 stopped-flow system fitted with a 75 W Xe/Hg lamp and monochromator for wavelength selection. Intrinsic tryptophan fluorescence was excited at 295 nm and emission monitored through a WG320 cut-off filter, while pyrene fluorescence was excited at 365 nm and emission monitored through a KV 398 nm cut-off filter. The stopped-flow transients were fitted to one or two exponentials as described previously by non-linear least squares curve fitting using the Kinetic Studio software (TgK Scientific). The reactant concentrations stated in the text and figures are those after 1:1 mixing in the stopped-flow spectrophotometer, unless stated otherwise. In some secondary data plots the plotted concentrations are those prior to mixing, which are then indicated as 'initial [X]'. All experiments were carried out at 20°C in 20 mM MOPS buffer containing 100 mM KCL, and 5 mM $MgCl_2$. In addition the buffer contained either 1 mM EGTA for measurements without calcium, or 1.1 mM EGTA and 1.2 mM $CaCl_2$ for measurements carried out in the presence of calcium.

Data Analysis

In the absence of actin the interaction of ATP and ADP with Myo1c was interpreted in terms of the 7-step mechanism for the myosin ATPase cycle (see Scheme 2) in which ATP binding to myosin occurs in two steps (a binding step and a protein conformational change followed by reversible ATP hydrolysis (35,36)). Pi release and ADP release then occur sequentially, each dissociation event preceded by a protein isomerisation. Our previous work established that ATP binding is accompanied by an increase in tryptophan fluorescence and there is no fluorescence change associated with ADP binding (14). We assume this fluorescence change is associated with the hydrolysis step because Myo1c has the conserved tryptophan at the end of the relay loop, which is known to signal the protein conformational change associated with switch II closure and the hydrolysis step in other myosins. The rate constant for the step $(k_{+3}+k_{-3})$ was inhibited 7-fold by calcium for $Myo1c^{1IQ}$-WT.

The results of the kinetic interaction of actin-$Myo1c^{1IQ}$ with nucleotide were interpreted in terms of the model we described previously for Myo1b (37) and Myo1c (5,14) (Scheme 1). The model assumes that acto-Myo1c exists in two conformations, A.M and A.M′, in the absence of nucleotide and that the interconversion between the two conformations is defined by the equilibrium constant K_α ($K_\alpha = k_{+\alpha} / k_{-\alpha}$). A.M′ represents the complex with the nucleotide pocket in the "closed" conformation which must isomerise into the "open-pocket" form, A.M, before nucleotide binding/release can occur. This isomerisation is believed to be coupled to a swing of the converter/IQ regions of the myosin motor domain. The ATP-induced dissociation of actin-myosin is biphasic. The fast phase represents ATP binding to A.M and the observed rate constant is hyperbolically dependent upon ATP concentration with $k_{obs,fast} = K_1k_{+2}[ATP]/(1+K_1[ATP])$.

The k_{obs} for the slow phase also shows hyperbolic dependence upon ATP concentration for $Myo1c^{1IQ}$-WT. This is unusual but reflects the fact that A.M′ is the predominant species present ($K_\alpha <1$). An exact solution to the ATP dependence of the slow phase is not possible but three regions of the ATP dependent behaviour of the slow phase can be described that depend upon the relative rate constants of ATP binding to A.M and the isomerisation of A.M′ to A.M. At very high [ATP] if $k_{-\alpha} \ll$ than the rate of ATP binding ($K_1k_{+2}[ATP]/(1+K_1[ATP])$) then every A.M′ that isomerises to A.M will bind ATP irreversibly and lead to dissociation of the myosin

from the complex. Under these conditions the k_{obs} has it maximal value and $k_{max,slow} = k_{+\alpha}$. For WT Myo1c then k_{+2} is more than ten times the maximum observed value of the slow phase and therefore the conditions are valid and $k_{max,slow} = k_{+\alpha}$.

At very low [ATP], such that $K_1[ATP] \ll 1$, the k_{obs} of ATP binding to A.M is $K_1 k_{+2}[ATP]$, and if this is slow compared to $k_{-\alpha} + k_{+\alpha}$ then only a single phase will be observed. The k_{obs} is then defined as $K_1 k_{+2}[ATP]/(1+ K_\alpha)$, the rate constant for ATP binding to A.M times the fraction of acto-Myo1c in the A.M conformation ($= 1/(1+ K_\alpha)$). This condition will always be fulfilled if the ATP concentration is low enough. The estimated value of $k_{-\alpha} + k_{+\alpha}$ for the WT is 20-25 s^{-1} independent of the presence of calcium and therefore this condition will be met at $[ATP] \ll 1$ mM.

If $k_{-\alpha} + k_{+\alpha}$ is of the same order as the fast phase then the observed slow phase will depend upon the relative rate constants of $k_{-\alpha}$ and the rate constant of ATP binding ($K_1 k_{+2}[ATP]/(1 +K_1[ATP])$). The half maximal value of the k_{obs} for the slow phase will be observed at the ATP concentration ($K_{0.5}$) when ($K_1 k_{+2}[ATP]/(1+K_1[ATP])) = k_{-\alpha}$. Since $k_{-\alpha}$ can be calculated from K_α (obtained from the relative amplitude of the fast and slow phases) and $k_{+\alpha} = k_{max, slow}$, then the value of $K_{0.5}$ can be predicted.

Two similar complexes are also assumed to exist in the presence of ADP, A.M.D and A.M′.D, with an open and closed nucleotide pocket, respectively. In the case of Myo1c^{1IQ}-WT the binding and release of ADP from A.M.D and A.M′.D cannot be distinguished because the rate constants governing ATP binding are slower than ADP release. The apparent ADP affinity can be estimated by measuring the ADP inhibition of the ATP-induced dissociation of acto-myosin. In the case of Myo1c^{1IQ}-WT, ADP is in rapid equilibrium with A.M and A.M′ on the time scale of the slow phase of the reaction. Thus, the slow phase, k_{obs}, is reduced with a hyperbolic dependence upon ADP concentration (independent of whether the ADP is premixed with the protein or the ATP) and $K_{0.5} = (K_{AD}/(1 + 1/K_\alpha)$, where K_{AD} is the affinity of A.M for ADP.

The observed behaviour of the ATP-induced dissociation reaction and the ADP inhibition of the slow phase are similar in the presence or absence of calcium, although the rate and equilibrium constants change. This is not the case for the fast phase of the dissociation reaction, which appears different in the presence and absence of ADP. The fast phase is small and difficult to characterise in the presence of ADP. When ADP is pre-incubated with the protein, the small amplitude of the fast phase decreases and cannot be measured at ADP concentrations above 5 μM. If ADP is pre-incubated with the ATP before mixing with protein then the observed behaviour is different in the presence vs. absence of calcium. In the absence of calcium the system behaves as though the ADP is in rapid equilibrium with A.M and A.M′, i.e., ADP binding and release is much faster than the rate constants for ATP binding ($K_1 k_{+2}[ATP]$) and ADP slows the k_{obs} with 50% inhibition when $[ADP] = K_{AD}$. If calcium is not present then the k_{obs} increases linearly with ADP concentration (38). This is consistent with the rate constant of ADP and ATP binding being of the same size and once ADP binds it is only released slowly. In this case, $k_{obs} = K_1 k_{+2}[ATP] + k_{-AD}[ADP]$, and in a plot of k_{obs} vs [ADP] the slope of the linear fit equals the second order binding rate constant k_{-AD} and the intercept equals $K_1 k_{+2}[ATP]$ (39,40). We therefore see a change in the behaviour from inhibition of ATP-induced dissociation of A.M by ADP in the absence of calcium to a 10-fold acceleration of the rate constant for ADP release (k_{+AD}) in calcium. Thus calcium alters the relative values of $K_1 k_{+2}[ATP]$ and k_{+AD}.

Results

There are two clear phases of the changes in pyrene fluorescence when ATP is rapidly mixed with pyr.actin-Myo1c^{1IQ}; a large slow phase and a small fast phase (50 % and 6 % amplitude,

respectively). The hyperbolic dependence of the fast phase in the absence of calcium was resolved (Figure 2) in contrast to our earlier work on the wild type, which could only resolve the data in the presence of calcium (14). The data in the presence of calcium are identical to this earlier work. The results are summarized in Table 3 and show that the removal of calcium accelerates the maximum k_{obs} (k_{+2}) from 19.6 s^{-1} to 41.2 s^{-1} while the $K_{0.5}$ ($1/K_1$) values decrease from 1.6 mM to 0.51 mM. Thus, calcium alters both the equilibrium constant for ATP binding and the isomerisation step, thought to be coupled to switch I movement (41). The steps sensitive to calcium are therefore: the ATP hydrolysis step, which is inhibited 7-fold by calcium; the ADP release from acto-myosin, which is activated 10-fold by calcium; and the ATP-induced dissociation of AM, in which the maximum rate constant is inhibited 2-fold and the ATP concentration for half maximal inhibition is increased 3-fold by calcium. This differs from all the other myosins that show calcium regulation. These have all been reported to have Ca^{2+}-dependence primarily of Pi-release and ADP binding and release events (22,42,43).

ATP-induced dissociation of the acto-Myo1c^{1IQ} alanine loop 1 chimeras

In the ATP-induced dissociation of acto-Myo1c the reaction remains biphasic for all the alanine loops (the transient for Myo1c^{1IQ}-8A is shown in Figure 3A) with the ratio of amplitudes independent of ATP concentration and a dominating slow phase. In the absence of calcium the fast phase was ~10% of the total amplitude for each construct and the addition of calcium reduced the fast phase by a factor of 2 at most, but since fast phase amplitudes are hard to define with precision the change is not significant. The k_{max} for the fast phase (k_{+2}) in the absence of calcium was unaffected by the change in the alanine loops (<20% reduction; Figure 3C). In the presence of calcium (data not shown) the 8A construct was unaffected, while the E/A (2-fold) and the R/A (5-fold) did show some acceleration of the reaction compared to WT. The slow phase k_{max} ($k_{+\alpha}$) was unaffected in the absence (Figure 3D) or presence of calcium except for the R/A construct which showed a 2-fold acceleration in the both the presence and absence of calcium. The results are summarised in Table 1.

Effect of ADP on the ATP-induced dissociation of acto-Myo1c^{1IQ} alanine loop 1 chimeras

To obtain an estimate of the affinity of ADP for acto-Myo1c for the loop 1 chimeras, the dissociation by ATP was monitored with increasing concentrations of ADP present (either by pre-incubating ADP with the protein or the ATP). Both experimental approaches produced biphasic transients for all mutants as observed with Myo1c^{1IQ}-WT (14), in both the presence and absence of ADP. If ADP binding is in rapid equilibrium with A.M and A.M′ the two experimental approaches will give the same results. This was true on the timescale of the slow phase, but not for the fast phase. The analysis of each phase will therefore be dealt with separately below. Typical pyrene fluorescence transients for the ATP-induced dissociation of acto-Myo1c^{1IQ} in the absence and presence of high ADP concentration (preincubated with acto-Myo1c) are shown in Figure 4A for Myo1c^{1IQ}-R/A (-Ca^{2+}) and 4B for Myo1c^{1IQ}-phasic (+Ca^{2+}).

Slow phase

If ADP is in rapid equilibrium with acto-Myo1c^{1IQ} on the time scale of the measurement, the two assays will give identical results for the k_{obs} of the slow phase (Figure 4C). As the ADP concentration was increased, the k_{obs} of the slow phase, which monitors the A.M′ species, was slowed for all constructs in a manner similar to that observed for Myo1c^{1IQ}-WT, both in the absence and presence of calcium. Hyperbolic fits provided the apparent ADP affinities (K_{app}) from which the K_{AD} were calculated. The alanine constructs all showed similar K_{app} and K_{AD} values as Myo1c^{1IQ}-WT, both in the absence (Figure 4C) and presence of calcium (with 10-fold weaker affinities in calcium; Figure 4D). The K_{AD} values are summarised in Table 2.

Fast phase

When ADP was pre-incubated with acto-Myo1c^{1IQ} the already small amplitude of the fast phase disappeared rapidly as ADP was added and no trace of a fast phase was determined at ADP > 5 μM, both with and without calcium making the analysis of the fast phase results unreliable in this experimental approach (see Figure 4A and 4B). This is consistent with the low values of K_{AD} calculated above and listed in Table 2.

When ADP was pre-incubated with ATP and then rapidly mixed with acto-Myo1c^{1IQ} the k_{obs} of the fast phase increased linearly with increasing ADP concentration. This diagnostic of a competition between ADP and ATP for the binding to acto-Myo1c^{1IQ} provides the 2nd order rate constant of ADP binding (slope = k_{-AD}) (data not shown). The R/A and E/A constructs had similar k_{-AD} values as WT (~1 $μM^{-1}s^{-1}$), while the 8A construct was 2-fold faster at 2.4 $μM^{-1}s^{-1}$. The experiment could only be completed reliably in the absence of calcium (the fast phase could not be determined reliably in calcium due to the small amplitudes).

Calculation of the ADP release constants (k_{+AD}) from the K_{AD} and ADP-binding rate constants in the chimeras in the absence of calcium showed values similar to those found for Myo1c^{1IQ}-WT at ~2 s^{-1} for Myo1c^{1IQ}-R/A and Myo1c^{1IQ}-E/A and slightly faster rate constants at ~4-5 s^{-1} for Myo1c^{1IQ}-8A (Table 2). In the presence of calcium, the ADP release rate constant for Myo1c^{1IQ}-WT was accelerated ~10-fold to 20 s^{-1}, while the values calculated for the alanine chimeras were accelerated between 5-7-fold (Table 2).

ATP-induced dissociation of acto-Myo1c^{1IQ}-tonic,-Myo1c^{1IQ}-phasic and -Myo1c^{1IQ}-G

When the ATP-induced dissociation of acto-Myo1c was performed with Myo1c^{1IQ}-tonic, Myo1c^{1IQ}-phasic and Myo1c^{1IQ}-G in the absence of calcium, the observed amplitudes were smaller than seen with Myo1c^{1IQ}-WT. The amplitudes in the absence of calcium of Myo1c^{1IQ}-phasic were as little as 1/5th of those for Myo1c^{1IQ}-WT, with 1.6 and 18 % for fast and slow phases, respectively. The smaller amplitudes make defining the maximal rate constant, k_{+2}, of the fast phase difficult. Despite the loss in total amplitude, the value for $K_{α}$ for Myo1c^{1IQ}-phasic was similar to Myo1c^{1IQ}-WT at 0.09 (Table 1) and this increased to 0.23 in the presence of calcium. The amplitudes obtained for Myo1c^{1IQ}-tonic were ~7 % and ~32 % of total fluorescence, for the fast and slow phases respectively, giving a value of $K_{α}$ of 0.21 in the absence of calcium and this decreased to 0.12 in the presence of calcium. The observed transients for Myo1c^{1IQ}-G are shown in Figure 3B and in the absence of calcium only a single phase could be distinguished with an amplitude of 13%. In the presence of calcium the slow phase had an amplitude of 13 %, while the fast-phase amplitude was 33 %, giving $K_{α}$ a value of 1.8 in the presence of calcium. Table 1 gives the values of $K_{α}$ for all the loop 1 chimeras in the presence and absence of calcium.

The k_{obs} values for the fast and slow phase of the ATP-induced dissociation in the absence of calcium for Myo1c^{1IQ}-tonic, Myo1c^{1IQ}-phasic and Myo1c^{1IQ}-G are shown in the secondary plots in Figures 3E and 3F. The plots for all constructs show hyperbolic dependence of the observed rate constants of the fast and slow phase on the ATP concentration. Hyperbolic fits of the data gave values for $k_{+α}$ (slow phase) for Myo1c^{1IQ}-tonic of 15 s^{-1}, ~8-fold faster than with Myo1c^{1IQ}-WT, while k_{+2} (fast phase) was slightly faster at 51 s^{-1}. In the presence of calcium the value for $k_{+α}$ was unchanged for Myo1c^{1IQ}-tonic, while k_{+2} was 2-fold faster than without calcium. In Myo1c^{1IQ}-phasic, $k_{+α}$ and k_{+2} were similar to Myo1c^{1IQ}-WT at ~2 s^{-1} and ~50 s^{-1}, respectively (Figure 3E). When calcium was present the value of $k_{+α}$ was reduced to 1.0 s^{-1}, while k_{+2} could not be determined reliably due to the very low amplitude. For Myo1c^{1IQ}-G the single-phase k_{obs} showed hyperbolic dependence on ATP concentration with a k_{max} of ~18 s^{-1} in the absence of calcium. In the presence of calcium the major phase had a

nearly identical k_{max} at 17.8 s^{-1} and a k_{max} at 5.7 s^{-1} for the slow component (data not shown). Assignments for the two phases for Myo1c^{1IQ}-G construct are not unambiguous since only a single phase is observed in the absence of calcium. In the presence of calcium two phases are observed and so the k_{max} for the fast phase is assigned to k_{+2} and the k_{max} of the slow phase to $k_{+\alpha}$ as previously. The single phase observed in the absence of calcium is problematic. It could be that K_α is <0.1 and so no fast phase is observed and thus the k_{max} value represents $k_{+\alpha}$ = 17 s^{-1}. This is much faster than any other value of $k_{+\alpha}$ observed (<4 s^{-1}), except that of Myo1c^{1IQ}-tonic (14 s^{-1}). Alternatively $k_{+\alpha}$ and k_{+2} are of the same order and the two phases cannot be resolved. We assign both values of 17 s^{-1} with K_α unresolved until we have further information. The values for k_{+2} and $k_{+\alpha}$ for all chimeras in the presence and absence of calcium are summarized in Table 1.

Effect of ADP on the ATP-induced dissociation of acto-Myo1c^{1IQ}-tonic, -Myo1c^{1IQ}-phasic and -Myo1c^{1IQ}-G

To obtain an estimate of the affinity of ADP for acto-Myo1c^{1IQ} of the smooth muscle myosin II and G-chimeras, the slow phase k_{obs} of the two experimental approaches (displacement and competition) were also plotted together as a function of ADP concentration and fitted to hyperbolae (Figure 4). The values of K_{app} in the absence of calcium for Myo1c^{1IQ}-tonic and Myo1c^{1IQ}-phasic were similar to WT at 22 μM (Figure 4E). When calcium was present the apparent affinity was weakened ~10-fold for Myo1c^{1IQ}-tonic (similar to WT), while Myo1c^{1IQ}-phasic, had an ~ 2-fold weaker K_{app} of 390 μM (Figure 4F). Since the K_α values of tonic and phasic were affected differently by the presence of calcium, the K_{AD} were very different as well: Myo1c^{1IQ}-phasic was similar to WT at 1.8 μM (-Ca^{2+}) and was weakened 40-fold by calcium, while the K_{AD} of Myo1c^{1IQ}-tonic only weakened 5-fold (from ~4 μM to ~18 μM).

Unlike Myo1c^{1IQ}-tonic and Myo1c^{1IQ}-phasic, the k_{obs} of Myo1c^{1IQ}-G at 0 μM ADP was 8-fold faster than for Myo1c^{1IQ}-WT and the apparent ADP affinity was at 48 μM, 2-fold weaker than for Myo1c^{1IQ}-WT (Figure 4E). When calcium was present Myo1c^{1IQ}-G did not produce usable data. Only single exponential transients were obtained, the rates and amplitudes of which showed little or no sensitivity to the concentration of ADP present, even at 250 μM, indicating only very weak affinity for ADP. The 2nd order ADP-binding rate constants determined from the fast phase k_{obs} for Myo1c^{1IQ}-tonic was similar to WT at 1.3 μM^{-1}s^{-1}; however, the ADP-binding rate constant could not be determined for Myo1c^{1IQ}-phasic or Myo1c^{1IQ}-G because the amplitudes of the fast phase were too small (for the purposes of the calculation we have assumed the value of k_{-AD} of these constructs is similar to that of the other constructs at ~ 1.0 μM^{-1}s^{-1}).

The ADP release constants (k_{+AD}) calculated from the K_{AD} and ADP-binding rate constants showed values in the absence of calcium for Myo1c^{1IQ}-phasic similar to those found for Myo1c^{1IQ}-WT and slightly faster rate constants for Myo1c^{1IQ}-tonic and Myo1c^{1IQ}-G at ~4-5 s^{-1} (Table 2). In the presence of calcium, the ADP release rate constant for Myo1c^{1IQ}-tonic showed only a 4-fold acceleration from 5 to 23 s^{-1} (WT was accelerated ~ 10-fold) and Myo1c^{1IQ}-phasic showed more than a 30-fold accelerated rate constant for ADP release in calcium (due to its much weaker K_{AD} in the presence of calcium). No data could be obtained for Myo1c^{1IQ}-G in calcium.

Nucleotide binding and release from the Myo1c^{1IQ} alanine loop 1 chimeras

The tryptophan fluorescence transients of ATP binding to the Myo1c^{1IQ} alanine loop 1 chimeras in the absence of actin were described by a single exponential with similar amplitudes as for WT (5-7 % reduced to 3-5 % in calcium; Figure 5A). The alanine loop constructs showed the same hyperbolic dependence of the k_{obs} as WT, both in the absence and presence of calcium,

with k_{max} ($=k_{+3}+k_{-3}$) values of ~45 s^{-1}, inhibited 6-8-fold when calcium was present (Table 3). In the presence of calcium the values of $k_{+\alpha}$ (~3 s^{-1}, Table 1) and $k_{+3}+k_{-3}$ (~6 s^{-1}) are similar, raising the possibility that $k_{+\alpha}$ is limited by a similar process as $k_{+3}+k_{-3}$. However, only $k_{+3}+k_{-3}$ is sensitive to calcium suggesting that they are not similar events.

Displacement of ADP from the $Myo1c^{1IQ}$ loop 1 chimeras by ATP was biphasic with amplitudes showing the same hyperbolic dependence on the ADP concentration present as reported previously for WT. The fast phase represents ATP binding to free Myo1c and the slow phase represents Myo1c with a bound ADP that must be released before ATP can bind (as shown in Figures 6A, 6B for $Myo1c^{1IQ}$-8A). Hyperbolic fits of the amplitudes found similarly tight ADP affinities (5-6 μM) for the alanine constructs as reported for WT (3.3 μM) (14). The k_{obs} of the slow phase, representing the rate constant of ADP release (k_{+D}), were again similar in the alanine constructs and WT at ~6 s^{-1}. In the presence of calcium the fast and slow phase could not be resolved, indicating that calcium slows ATP binding to a similar value as the rate constant of ADP release, but leaving k_{+D} independent of calcium at ~4 s^{-1} (Table 2).

ATP binding to $Myo1c^{1IQ}$-tonic, $Myo1c^{1IQ}$-phasic and $Myo1c^{1IQ}$-G in the absence of actin

ATP binding to $Myo1c^{1IQ}$-tonic, $Myo1c^{1IQ}$-phasic and $Myo1c^{1IQ}$-G differed from the results obtained with $Myo1c^{1IQ}$-WT and the alanine chimeras in so far that the transients of the tonic, phasic and G constructs displayed evidence of a small additional slow phase upon ATP binding in the absence of calcium, but not in its presence (as observed in $Myo1c^{1IQ}$-WT). Figure 5B shows typical transients observed upon binding of 1 mM ATP to $Myo1c^{1IQ}$-G in the absence and presence of calcium. The origin of this additional slow phase is unknown and could not be resolved any further in $Myo1c^{1IQ}$-tonic and $Myo1c^{1IQ}$-phasic due to the very small amplitude (< 0.5 %). The k_{max} values obtained for the fast phase of these chimeras were 1.5-2-fold faster than found for the wild type, both in the absence and presence of calcium, as shown in the secondary plots of ATP binding in Figures 5C and 5D, respectively (see also Table 3). The $1/K_1$ values were 75-100 μM for the three chimeras, half the value observed for $Myo1c^{1IQ}$-WT. Addition of calcium reduced $1/K_1$ ~3-fold for $Myo1c^{1IQ}$-tonic (similar in value to $Myo1c^{1IQ}$-WT) and much less for $Myo1c^{1IQ}$-phasic and $Myo1c^{1IQ}$-G. The presence of calcium reduced the k_{max} 4-5 fold for $Myo1c^{1IQ}$-tonic and $Myo1c^{1IQ}$-phasic and ~6 fold for the $Myo1c^{1IQ}$-G, similar to the wild-type results (see Table 3). In the case of $Myo1c^{1IQ}$-G the second phase was reasonably well resolved, both in the absence and presence of calcium, with an amplitude of ~1.5 % and k_{max} value of ~9 s^{-1} and ~3 s^{-1}, respectively. It is assumed here that the fast phase corresponds to the hydrolysis rate constant observed for the other chimeras, since the amplitude is of a similar size (6 %) and behaves in the same manner with $K_{0.5}$ and K_1k_{+2} values comparable to the tonic and phasic chimeras. However, the binding of ATP to many myosins occurs in two distinct steps, first the partial closing of switch II, accompanied by an enhancement in tryptophan fluorescence (reported by W^{510} in skeletal muscle myosin II and W^{433} in Myo1c), followed by the hydrolysis step, which fully closes switch II (44, 45). In most myosins this first step cannot be resolved experimentally. The two phases observed here in $Myo1c^{1IQ}$-G on ATP binding could therefore represent these two reaction steps: switch II closing at ~80 s^{-1} (fast phase) followed by much slower hydrolysis at ~10 s^{-1} (slow phase).

ADP displacement from $Myo1c^{1IQ}$-tonic, $Myo1c^{1IQ}$-phasic and $Myo1c^{1IQ}$-G

When ADP was displaced from $Myo1c^{1IQ}$-tonic, $Myo1c^{1IQ}$-phasic and $Myo1c^{1IQ}$-G by a large excess of ATP the results differed from those of the WT and the alanine constructs. In the absence of calcium the tryptophan transients of ADP displacement from these chimeras were also described by two exponentials (as observed for WT), however the amplitude changed for these constructs as ADP was increased. For $Myo1c^{1IQ}$-tonic pre-incubation with increasing ADP concentrations in the absence of calcium reduced the total amplitude of the tryptophan fluorescence transient from 5% to 2-3%. The fast amplitude (with $k_{obs} = $ ~80 s^{-1}) decreased

towards zero and could be described by a hyperbola with a K_D of 9.2 μM (Figure 6C). The amplitude of the slow phase was too small (<2%) to allow reliable analysis of the concentration dependence, but the k_{obs} (= k_{+D}) was ~7 s^{-1}, similar to that seen with Myo1c^{1IQ}-WT. The tonic loop therefore weakens the affinity of Myo1c for ADP 3-fold compared to Myo1c^{1IQ}-WT in the absence of calcium, but has little effect on the rate constant for ADP release (k_{+D}).

For Myo1c^{1IQ}-phasic the total observed amplitude of the reaction was too small (2-3%) to allow the two phases to be distinguished from each other, hence no K_D could be determined. However, working at very high ATP concentration (10 mM) in the presence of 50 μM ADP, the ADP release rate constant (k_{+D}) from Myo1c^{1IQ}-phasic could be measured as 37 s^{-1} (compared to 60 s^{-1} for $k_{+3}+k_{-3}$) with an amplitude of 2%. The results are consistent with a relatively weak affinity of ADP for Myo1c^{1IQ}-phasic and a 6-fold faster ADP-dissociation constant compared to Myo1c^{1IQ}-WT.

The addition of 0.5 mM ATP to Myo1c^{1IQ}-G showed two phases in the tryptophan fluorescence transient even in the absence of ADP as shown in the secondary plots of Figure 5C. Pre-incubating Myo1c^{1IQ}-G with ADP (2-100 μM) resulted in the k_{obs} of the fast phase slowing from 71 s^{-1} (at zero ADP) to ~25-30 s^{-1} (at high ADP, as shown in Figure 6D) and this slowing of the observed rate constant was accompanied by a loss in amplitude of the fast phase from 6 to ~ 4 %. The slow-phase k_{obs} and amplitudes were not very well defined (~2.5 %), but neither showed any sensitivity to ADP. A hyperbolic fit of the fast-phase k_{obs} values gave a $K_{0.5}$ of 7.9 ± 3.0 μM. This result is indicative of a different type of mechanism at work in Myo1c^{1IQ}-G. The data are compatible with an ADP affinity of ~8 μM and an ADP-release rate constant (k_{+D}) of 25-30 s^{-1}, indicating that displacement of ADP from myosin is at fast equilibrium compared to ATP binding in this chimera.

Repeating the ADP displacement measurement in the presence of calcium was limited by the small amplitudes of the transients with Myo1c^{1IQ}-phasic and Myo1c^{1IQ}-G and was only possible for Myo1c^{1IQ}-tonic (Figure 7). As the ADP concentration was increased from 0 to 50 μM the observed fast-phase amplitude of Myo1c^{1IQ}-tonic decreased from ~5 % to 1 % (Figure 7B) and at the same time the k_{obs} slowed from ~13 to 4 s^{-1} (Figure 7A). A hyperbolic fit of the k_{obs} and amplitude data gave $K_{0.5}$ values of ~18 and 11 μM, respectively. Increasing the ATP concentration to 10 mM (with ADP at 50 μM) gave an unchanged amplitude and a k_{obs} of 18 s^{-1} (similar to the k_{max} for ATP binding) suggesting that the ADP-release rate constant (k_{+D}) is greater than 18 s^{-1} in the presence of calcium. This suggests that the displacement of ADP from Myo1c^{1IQ}-tonic is at fast equilibrium compared to the maximal rate constant of ATP binding (on the timescale of the measurement) and the ADP affinity of Myo1c^{1IQ}-tonic is weakened up to 2-fold in calcium, resulting in a 2-fold acceleration of the ADP-release rate constant. This behaviour stands in contrast to results obtained for the alanine chimeras or Myo1c^{1IQ}-WT, where the K_D appeared little changed by calcium (Table 2).

Steady-state ATPase activity

As previously observed (7,14,42) the basal ATPase of Myo1c is very low (≪ 0.1 s^{-1}) and relatively insensitive to calcium. The Myo1c^{1IQ} constructs show similar low basal ATPase except for Myo1c^{1IQ}-phasic and Myo1c^{1IQ}-G which had elevated basal ATPase activity at high, but not low, calcium concentrations with V_0 values of 0.23 and 0.48 s^{-1}, respectively. The steady-state actin-activated Mg^{2+}-ATPase activity of Myo1c^{1IQ}-WT is shown in Figure 8. The ATPase activity was relatively low with little calcium sensitivity over the range of pCa 4.6 - 8.9 (V_{max} 2 ± 0.26 s^{-1} at pCa 4.6; 1.8 ± 0.19 s^{-1} at pCa 8.9). All of the mutants were activated with increasing amounts of actin and their behaviour was not dramatically different from Myo1c^{1IQ}-WT. Exceptions were that the V_{max} of Myo1c^{1IQ}-tonic was higher than Myo1c^{1IQ}-WT at 3.36 ± 0.08 s^{-1} and the K_m of Myo1c^{1IQ}-G at 0.28 ± 0.04 μM at pCa 4.6 was

70-fold lower than Myo1c^{1IQ}-WT (20 ± 7 μM) and Myo1c^{1IQ}-phasic with very low V_{max} and K_m values.

The same trend was observed for the constructs with 2 IQs and an incorporated SAH domain (data not shown) indicating that modification of the LCBD by incorporation of a single α-helix did not adversely affect the enzymatic activity of the Myo1c motor domain.

In vitro translocation of actin by Myo1c mutants

The yield of expressed protein from insect cells for the 1-IQ forms of Myo1c exceeds that of expressed full-length Myo1c in our hands; however, the light-chain-binding domain (LCBD), which acts as a lever arm and therefore affects the maximum rate of motility (46), is short in the 1-IQ form. To investigate the ability of the Myo1c loop 1 mutants to translocate actin filaments *in vitro*, we prepared fusion proteins of wild-type Myo1c and the loop 1 mutants, phasic, tonic and G, with a recently recognized structural element found in myosin X. Myosin X contains a 36-residue sequence that forms a single α-helix (or SAH) (47). We reasoned that addition of the SAH domain to the LCBD of Myo1c would act as an extended artificial lever arm much the same way that α-actinin repeats do (47) and make the constructs suitable for use in *in vitro* motility assays. In 1 mM EGTA Myo1c^{SAH}-WT translocated actin filaments at 12 ± 4 nm/sec (353 filaments) (Table 4). This is not inconsistent with the previously determined rate for baculovirus-expressed full-length rat Myo1c of 30 nm/sec (48). The motility of Myo1c^{SAH}-WT was twice the rate of Myo1c^{SAH}-phasic (5 ± 3 nm/sec, 318 filaments) and about half that of Myo1c^{SAH}-tonic (22 ± 7 nm/sec, 587 filaments) and Myo1c^{SAH}-G (29 ± 7 nm/sec, 455 filaments). The data should be viewed as preliminary because the ideal splicing point for fusing the IQ domain with the SAH domain has not yet been explored; however, the values for V_{max} of the ATPase data for these constructs show the same relationship and were about 70% of the values listed in Figure 8 for the 1IQ constructs.

Discussion

In this study we investigated the role of loop 1 in defining the biochemical properties of Myo1c. Loop 1 influences the rate constant of ADP release in a number of different myosins and the nature of the ADP release from acto-myosin is a key element in defining the mechano-chemical characteristics of myosins (23,26,27). For example, ADP release is coupled to a small swing of the motor domain in the same direction as the Pi-coupled power stroke of several myosins and this is thought to be central to the load sensitivity of the ADP-release step (5,37,38,49). ADP release has also been proposed to limit the velocity of low duty ratio myosins, where it does not limit the ATPase cycle (17). In the case of Myo1c we have recently shown that ADP release is also calcium sensitive, thereby providing a mechanism in which calcium could alter the duty ratio of this myosin (14). Thus, understanding how the ADP-release rate is defined for a given myosin is a core issue in understanding the mechano-chemistry of each myosin. In addition, if a simple way to modulate the ADP release by small changes in the sequence of loop 1 could be defined, these same myosins could be expressed in mice to test how mechano-chemical properties are modulated *in vivo*. The results presented here show that modifying loop 1 alters the ADP-release characteristics of Myo1c; however, as for myosin II the resulting properties cannot be easily predicted from sequence alone.

We show here that the length of loop 1 may be important as suggested previously (26) whereas exchanging residues in loop 1 for alanine residues, individually or as a group of 8, had very little effect on any of the parameters measured here including calcium sensitivity. In most cases the measured parameters were within 10-20% of the wild-type values. The exceptions were the ATPase V_{max} values of Myo1c^{1IQ}-8A, which were ~40 % higher at both high and low calcium and the rate constant of ADP release from A.M.D, k_{+AD}, which was elevated by ~2 fold in the absence of calcium. This increase in k_{+AD} is consistent with ADP release being rate

limiting for the ATPase cycle at low calcium. In contrast, the rate constant for the ATP hydrolysis step of Myo1c^{1IQ}-8A, which is considered to be partially rate limiting for the ATPase cycle in the presence of calcium, was altered <10% compared to WT.

Overall, the alanine constructs provided little evidence of a specific role of the amino acid side chains in the wild-type loop 1, even for the proline side chains, which are expected to provide restricted flexibility in the loop structure. In contrast, shortening the loop to a single glycine or extending it with the longer loops found in smooth muscle myosin II produced significant changes in the behaviour of the constructs.

The best behaved mutant of the second group of constructs – in that it showed no major alteration in overall properties - was Myo1c^{1IQ}-tonic. For this construct the K_m for actin values was relatively unaffected, but V_{max} values were elevated by ~30% at low calcium and almost 2-fold at high calcium (Figure 8). A similar increase of ~2-fold was also observed for the velocity of the SAH constructs in motility assays (Table 4). If the hydrolysis rate constant is contributing to limiting the V_{max} values at high calcium in Myo1c^{1IQ}-tonic, then an increase in the rate constant of the hydrolysis step ($k_{+3}+k_{-3}$) is expected and a 2.5-fold increase was indeed observed. The increase in the rate constant of the hydrolysis step ($k_{+3}+k_{-3}$) was smaller at low calcium at ~ 60 %. The increase in the rate constant of hydrolysis at high calcium is consistent with a contribution of the hydrolysis step to the ATPase activity; however, this is unlikely to be direct since the hydrolysis rate constant is ~ 5 times the V_{max} value for this construct even at high calcium (3 times for WT).

At low calcium the ADP-release rate constant is thought to limit the ATPase activity. Whereas the ADP release rate constant (k_{+AD}) and the V_{max} were similar for the WT, the ADP release for Myo1c^{1IQ}-tonic was up to twice the value of the V_{max} (and a little less in the presence of calcium). This difference is made clear when the ratio of the $k_{+AD}/(k_{+3}+k_{-3})$ in the absence of calcium for WT and tonic (2.1/44 = 0.048 and 4.9/72.3 = 0.067, respectively) is compared with the same values in the presence of calcium (20.3/6.3 = 3.2 and 23/15 = 1.53, respectively).

Other differences in the kinetic parameters determined for Myo1c^{1IQ}-tonic were variable. Notable is that the $k_{+\alpha}$ values were 5-fold faster with little impact on K_{α} and the ADP affinity for myosin (without actin) was 3-fold weaker with little effect on the rate constant of ADP release (k_{-D}). The Myo1c^{1IQ}-phasic construct had a higher basal ATPase, lower V_{max} values (30-50% of WT), and the velocities measured in the motility assays were also about 50% of the WT (25% of those of the tonic construct) (see Figure 8 and Table 4). It should be noted that many of the transient kinetic parameters measured here were much harder to evaluate for Myo1c^{1IQ}-phasic since the amplitudes of the fluorescence changes were much smaller in most cases. Note that in the absence of actin, the affinity of ADP for myosin could not be determined, while the hydrolysis step ($-Ca^{2+}$) was 1.5- to 2-fold faster, despite a lower V_{max}. In the presence of actin $k_{+\alpha}$ and K_{α} were not strongly affected by calcium, while the K_{AD} in the presence of calcium was weakened 5-fold, but no change was observed in the absence of calcium. This is interpreted as a large (4-5-fold) increase in k_{+AD}, which only occurs in the presence of calcium.

For the Myo1c^{1IQ}-G construct the basal ATPase was also higher, although the V_{max} values were similar to WT with a much lower apparent affinity for actin. The unchanged V_{max} values were not reflected in the motility data, which showed 2.5-fold faster velocities than WT (see Figure 8 and Table 4). Other major changes for Myo1c^{1IQ}-G were a biphasic fluorescence change in the absence of actin, while single-phase fluorescence transients were observed in the presence of actin ($-Ca^{2+}$).

In summary, each of these three constructs showed a distinct set of properties and no general pattern was observed. All of the properties assayed here are therefore potentially modulated,

either directly or indirectly, by the structure of the loop 1. A similar set of constructs in the Myo1b backbone also resulted in a wide range of distinct responses, albeit differing to the ones observed here with Myo1c^{1IQ} (22). The native loops of Myo1b and Myo1c are of similar size but different sequence (Figure 1A). In the Myo1b backbone the loss of either charged residue or the change to a series of alanine residues gave distinct properties to the myosin, including changes to K_α, K_{AD} and the calcium sensitivity of the two parameters. That the effects of a mutation in one myosin do not necessarily correlate with the same mutation in different backgrounds has been seen with other myosins, notably in a recent study of the R403Q mutation in myosin II, which is associated with familial cardiomyopathy (31). This is also true of loop 1 in smooth muscle myosin II where the longer phasic loop 1 is associated with a weaker ADP affinity in the presence of actin (K_{AD}) and a faster velocity of muscle shortening (26). Here we observe little difference in K_{AD} in the absence of calcium (2-fold tighter for phasic than tonic), but 5-fold weaker for phasic in the presence of calcium. In Myo1b the phasic loop gave a 2-fold tighter K_{AD} (2 μM) than for tonic (5.8 μM) in the presence of calcium and the difference disappeared in the absence of calcium, where for both tonic and phasic loops the K_{AD} affinity was very tight at 0.7 μM.

Thus we conclude that for the surface loops explored to date, the parent myosin dominates the behaviour and loop 1 modulates the properties of the parent myosin. The loops themselves do not confer predictable properties on the parent myosin and their roles can only be defined in the context of the myosin. This is consistent with the loop altering the connecting structural elements (the helices connecting to the P-loop and switch I) and thereby modulating the myosin behaviour, rather than the loop having specific interactions with other parts of the myosin molecule.

Acknowledgments

References

1. Foth BJ, Goedecke MC, Soldati D. New insights into myosin evolution and classification. Proc Natl Acad Sci U S A 2006;103:3681–3686. [PubMed: 16505385]

2. Odronitz F, Kollmar M. Drawing the tree of eukaryotic life based on the analysis of 2,269 manually annotated myosins from 328 species. Genome Biol 2007;8:R196. [PubMed: 17877792]

3. Coluccio, LM. Myosins, A Superfamily of Molecular Motors. Springer; Dordrecht, The Netherlands: 2008a.

4. Mermall V, Post PL, Mooseker MS. Unconventional myosins in cell movement, membrane traffic, and signal transduction. Science 1998;279:527–533. [PubMed: 9438839]

5. Batters C, Arthur CP, Lin A, Porter J, Geeves MA, Milligan RA, Molloy JE, Coluccio LM. Myo1c is designed for the adaptation response in the inner ear. Embo J 2004a;23:1433–1440. [PubMed: 15014434]

6. Sokac AM, Schietroma C, Gundersen CB, Bement WM. Myosin-1c couples assembling actin to membranes to drive compensatory endocytosis. Dev Cell 2006;11:629–640. [PubMed: 17084356]

7. Stauffer EA, Scarborough JD, Hirono M, Miller ED, Shah K, Mercer JA, Holt JR, Gillespie PG. Fast adaptation in vestibular hair cells requires myosin-1c activity. Neuron 2005;47:541–553. [PubMed: 16102537]

8. Barylko B, Jung G, Albanesi JP. Structure, function, and regulation of myosin 1C. Acta Biochim Pol 2005;52:373–380. [PubMed: 15933767]

9. Gillespie PG, Cyr JL. Calmodulin binding to recombinant myosin-1c and myosin-1c IQ peptides. BMC Biochem 2002;3:31. [PubMed: 12453307]

10. Reizes O, Barylko B, Li C, Sudhof TC, Albanesi JP. Domain structure of a mammalian myosin I beta. Proc Natl Acad Sci U S A 1994;91:6349–6353. [PubMed: 8022785]

11. Bose A, Guilherme A, Robida SI, Nicoloro SM, Zhou QL, Jiang ZY, Pomerleau DP, Czech MP. Glucose transporter recycling in response to insulin is facilitated by myosin Myo1c. Nature 2002;420:821–824. [PubMed: 12490950]

12. Bose A, Robida S, Furcinitti PS, Chawla A, Fogarty K, Corvera S, Czech MP. Unconventional myosin Myo1c promotes membrane fusion in a regulated exocytic pathway. Mol Cell Biol 2004;24:5447–5458. [PubMed: 15169906]

13. Yip MF, Ramm G, Larance M, Hoehn KL, Wagner MC, Guilhaus M, James DE. CaMKII-Mediated Phosphorylation of the Myosin Motor Myo1c Is Required for Insulin-Stimulated GLUT4 Translocation in Adipocytes. Cell Metab 2008;8:384–398. [PubMed: 19046570]

14. Adamek N, Coluccio LM, Geeves MA. Calcium sensitivity of the cross-bridge cycle of Myo1c, the adaptation motor in the inner ear. Proc Natl Acad Sci U S A 2008;105:5710–5715. [PubMed: 18391215]

15. Fisher AJ, Smith CA, Thoden J, Smith R, Sutoh K, Holden HM, Rayment I. Structural studies of myosin:nucleotide complexes: a revised model for the molecular basis of muscle contraction. Biophys 1995;J 68:19S–26S. discussion 27S-28S.

16. Geeves MA, Holmes KC. Structural mechanism of muscle contraction. Annu Rev Biochem 1999;68:687–728. [PubMed: 10872464]

17. Nyitrai M, Rossi R, Adamek N, Pellegrino MA, Bottinelli R, Geeves MA. What limits the velocity of fast-skeletal muscle contraction in mammals? J Mol Biol 2006;355:432–442. [PubMed: 16325202]

18. Somlyo AV, Khromov AS, Webb MR, Ferenczi MA, Trentham DR, He ZH, Sheng S, Shao Z, Somlyo AP. Smooth muscle myosin: regulation and properties. Philos Trans R Soc Lond B Biol Sci 2004;359:1921–1930. [PubMed: 15647168]

19. Nyitrai M, Stafford WF, Szent-Gyorgyi AG, Geeves MA. Ionic interactions play a role in the regulatory mechanism of scallop heavy meromyosin. Biophys J 2003;85:1053–1062. [PubMed: 12885652]

20. Rovner AS, Fagnant PM, Trybus KM. Phosphorylation of a single head of smooth muscle myosin activates the whole molecule. Biochemistry 2006;45:5280–5289. [PubMed: 16618116]

21. Wendt T, Taylor D, Trybus KM, Taylor K. Three-dimensional image reconstruction of dephosphorylated smooth muscle heavy meromyosin reveals asymmetry in the interaction between myosin heads and placement of subfragment 2. Proc Natl Acad Sci U S A 2001;98:4361–4366. [PubMed: 11287639]

22. Clark R, Ansari MA, Dash S, Geeves MA, Coluccio LM. Loop 1 of transducer region in mammalian class I myosin, Myo1b, modulates actin affinity, ATPase activity, and nucleotide access. J Biol Chem 2005;280:30935–30942. [PubMed: 15980431]

23. Spudich JA. How molecular motors work. Nature 1994;372:515–518. [PubMed: 7990922]

24. Rovner AS, Freyzon Y, Trybus KM. An insert in the motor domain determines the functional properties of expressed smooth muscle myosin isoforms. J Muscle Res Cell Motil 1997;18:103–110. [PubMed: 9147986]

25. Somlyo AP. Myosin isoforms in smooth muscle: how may they affect function and structure? J Muscle Res Cell Motil 1993;14:557–563. [PubMed: 8126215]

26. Sweeney HL, Rosenfeld SS, Brown F, Faust L, Smith J, Xing J, Stein LA, Sellers JR. Kinetic tuning of myosin via a flexible loop adjacent to the nucleotide binding pocket. J Biol Chem 1998;273:6262–6270. [PubMed: 9497352]

27. Kurzawa-Goertz SE, Perreault-Micale CL, Trybus KM, Szent-Gyorgyi AG, Geeves MA. Loop I can modulate ADP affinity, ATPase activity, and motility of different scallop myosins. Transient kinetic analysis of S1 isoforms. Biochemistry 1998;37:7517–7525. [PubMed: 9585566]

28. Murphy CT, Spudich JA. Dictyostelium myosin 25-50K loop substitutions specifically affect ADP release rates. Biochemistry 1998;37:6738–6744. [PubMed: 9578557]

29. Goodson HV, Warrick HM, Spudich JA. Specialized conservation of surface loops of myosin: evidence that loops are involved in determining functional characteristics. J Mol Biol 1999;287:173–185. [PubMed: 10074415]

30. Dominguez R, Freyzon Y, Trybus KM, Cohen C. Crystal structure of a vertebrate smooth muscle myosin motor domain and its complex with the essential light chain: visualization of the pre- power stroke state. Cell 1998;94:559–571. [PubMed: 9741621]

31. Lowey S, Lesko LM, Rovner AS, Hodges AR, White SL, Low RB, Rincon M, Gulick J, Robbins J. Functional effects of the hypertrophic cardiomyopathy R403Q mutation are different in an alpha- or beta-myosin heavy chain backbone. J Biol Chem 2008;283:20579–20589. [PubMed: 18480046]

32. Perreault-Micale C, Shushan AD, Coluccio LM. Truncation of a mammalian myosin I results in loss of Ca^{2+}-sensitive motility. J Biol Chem 2000;275:21618–21623. [PubMed: 10777479]

33. Pollard TD. Myosin purification and characterisation. Methods Cell Biol 1982;24:333–371. [PubMed: 6212751]

34. Sellers JR, Cuda G, Wang F, Homsher E. Myosin-specific adaptations of the motility assay. Methods Cell Biol 1993;39:23–49. [PubMed: 8246800]

35. Bagshaw CR, Trentham DR. The characterization of myosin-product complexes and of product-release steps during the magnesium ion-dependent adenosine triphosphatase reaction. Biochem J 1974;141:331–349. [PubMed: 4281653]

36. Trentham DR, Eccleston JF, Bagshaw CR. Kinetic analysis of ATPase mehanisms. Quarterly Rev Biophys 1976;9:217–281.

37. Geeves MA, Perreault-Micale C, Coluccio LM. Kinetic analyses of a truncated mammalian myosin I suggest a novel isomerization event preceding nucleotide binding. J Biol Chem 2000;275:21624–21630. [PubMed: 10781577]

38. Siemankowski RF, Wiseman MO, White HD. ADP dissociation from actomyosin subfragment 1 is sufficiently slow to limit the unloaded shortening velocity in vertebrate muscle. Proc Natl Acad Sci U S A 1985;82:658–662. [PubMed: 3871943]

39. Robblee JP, Cao W, Henn A, Hannemann DE, De La Cruz EM. Thermodynamics of nucleotide binding to actomyosin V and VI: a positive heat capacity change accompanies strong ADP binding. Biochemistry 2005;44:10238–10249. [PubMed: 16042401]

40. Robblee JP, Olivares AO, de la Cruz EM. Mechanism of nucleotide binding to actomyosin VI: evidence for allosteric head-head communication. J Biological Chemistry 2004;279:38608–38617.

41. Kovacs M, Malnasi-Csizmadia A, Woolley RJ, Bagshaw CR. Analysis of nucleotide binding to Dictyostelium myosin II motor domains containing a single tryptophan near the active site. J Biological Chemistry 2002;277:28459–28467.

42. Nyitrai M, Szent-Gyorgyi AG, Geeves MA. A kinetic model of the cooperative binding of calcium and ADP to scallop (Argopecten irradians) heavy meromyosin. Biochem J 2002;365:19–30. [PubMed: 12071838]

43. Olivares AO, Chang W, Mooseker MS, Hackney DD, De La Cruz EM. The tail domain of myosin Va modulates actin binding to one head. J Biological Chemistry 2006;281:31326–31336.

44. Malnasi-Csizmadia A, Pearson DS, Kovacs M, Woolley RJ, Geeves MA, Bagshaw CR. Kinetic resolution of a conformational transition and the ATP hydrolysis step using relaxation methods with a Dictyostelium myosin II mutant containing a single tryptophan residue. Biochemistry 2001;40:12727–12737. [PubMed: 11601998]

45. Malnasi-Csizmadia A, Woolley RJ, Bagshaw CR. Resolution of conformational states of Dictyostelium myosin II motor domain using tryptophan (W501) mutants: implications for the open-closed transition identified by crystallography. Biochemistry 2000;39:16135–16146. [PubMed: 11123942]

46. Uyeda TQ, Abramson PD, Spudich JA. The neck region of the myosin motor domain acts as a lever arm to generate movement. Proc Natl Acad Sci U S A 1996;93:4459–4464. [PubMed: 8633089]

47. Knight PJ, Thirumurugan K, Xu Y, Kalverda AP, Stafford WFI, Sellers JR, Peckham M. The predicted coiled-coil domain of myosin 10 forms a novel elongated domain that lengthens the head. J Biol Chem 2005;280:34702–34708. [PubMed: 16030012]

48. Zhu T, Sata M, Ikebe M. Functional expression of mammalian myosin I beta: analysis of its motor activity. Biochemistry 1996;35:513–522. [PubMed: 8555222]

49. Coluccio LM, Geeves MA. Transient kinetic analysis of the 130-kDa myosin I (MYR-1 gene product) from rat liver. A myosin I designed for maintenance of tension? J Biol Chem 1999;274:21575–21580. [PubMed: 10419463]

Abbreviations

A	actin
BSA	bovine serum albumin
D	ADP
F-actin	filamentous actin
M	myosin
Myo1b	myosin 1b
Myo1c	myosin 1c
PCR	polymerase chain reaction
Pyrene	pyr, N-(l-pyrenyl) iodoacetamide
SAH	single alpha helix
T	ATP
WT	wild type

(A)

```
                  P-loop    HHHHHHHHHHHHH   Loop 1           HHHHHHHHHHHHHHHHHHHHHHHHHHHHH  Switch 1
   Myo1c   ISGESGAGKTEATKRLLQFYAETCPAPERGGA-------------VRDRLLQSNPVLEAFGNAKTLRNDNSSRFGKYMDVQF 171
   MyoE    ISGESGAGKTEASKKIMQFLTFVSSNQS-------------PNGERISKMLLDSNPLLEAFGNAKTLRNDNSSRFGKYMEMQF 168
   Myo1b   ITGESGAGKTEASKLVMSYVAAVCGKGAEVN-------------QVKEQLLQSTPVLEAFGNAKTVRNDNSSRFGKYMDIEF 174
   phasic  CTGESGAGKTENTKKVIQYLAVVASSHKGKKDTSITQGPSFSYGELEKQLLQANPILEAFGNAKTVKNDNSSRFGKFIRINF 155
   tonic   CTGESGAGKTENTKKVIQYLAVVASSHKGKKDTSIT-------GELEKQLLQANPILEAFGNAKTVKNDNSSRFGKFIRINF 150
   MyoII   ITGESGAGKTENTKKVIQYLASVAGRNQANGS-----------GVLEQQILQANPILEAFGNAKTTRNNNSSRFGKFIEIQF 146
           :*********  :*  ::.:  : ..               :  .  :*::.*:********** :*:*******:: ::*
```

(B)

Myo1c^{1IQ} construct	Loop 1 sequence
Myo1c^{1IQ}-WT	PAPERGGA
Myo1c^{1IQ}-R/A	PAPE<u>A</u>GGA
Myo1c^{1IQ}-E/A	PAP<u>A</u>RGGA
Myo1c^{1IQ}-8A	<u>AAAAAAAA</u>
Myo1c^{1IQ}-tonic	SHKGKKDTSIT
Myo1c^{1IQ}-phasic	SHKGKKDTSITQGPSFSY
Myo1c^{1IQ}-G	G

Figure 1.
A, sequence alignment of the loop 1 region (underlined) in the myosin head starting with the P-loop (bold) and ending after switch-1 (bold). Shown are the sequences of rat Myo1c, *Dictyostelium* MyoE, rat Myo1b, chicken phasic smooth muscle myosin II, rabbit tonic smooth muscle myosin II and *Dictyostelium* myosin II. Secondary structure assignments were made using the structure of the motor domain of *Dictyostelium* MyoE (1LKX) as a guide. Symbols: *, residues identical in all sequences; :, conserved substitutions; ., semi-conserved substitutions; H, helical region. *B*, list of loop 1 constructs used in study.

Figure 2.
ATP-induced dissociation of pyr.acto-Myo1c^{1IQ}-WT in the absence and presence of calcium. Plots of the fast phase k_{obs} of the pyrene fluorescence transient as a function of ATP concentration (with and without calcium). Data were fitted to a hyperbolae to obtain k_{max} and $K_{0.5}$ values: -Ca^{2+}: $k_{max} = 41.2 \pm 2.3$ s^{-1}, $K_{0.5} = 0.51 \pm 0.1$ mM; +Ca^{2+}: $k_{max} = 19.6 \pm 4.1$ s^{-1}, $K_{0.5} = 1.66 \pm 1.0$ mM.
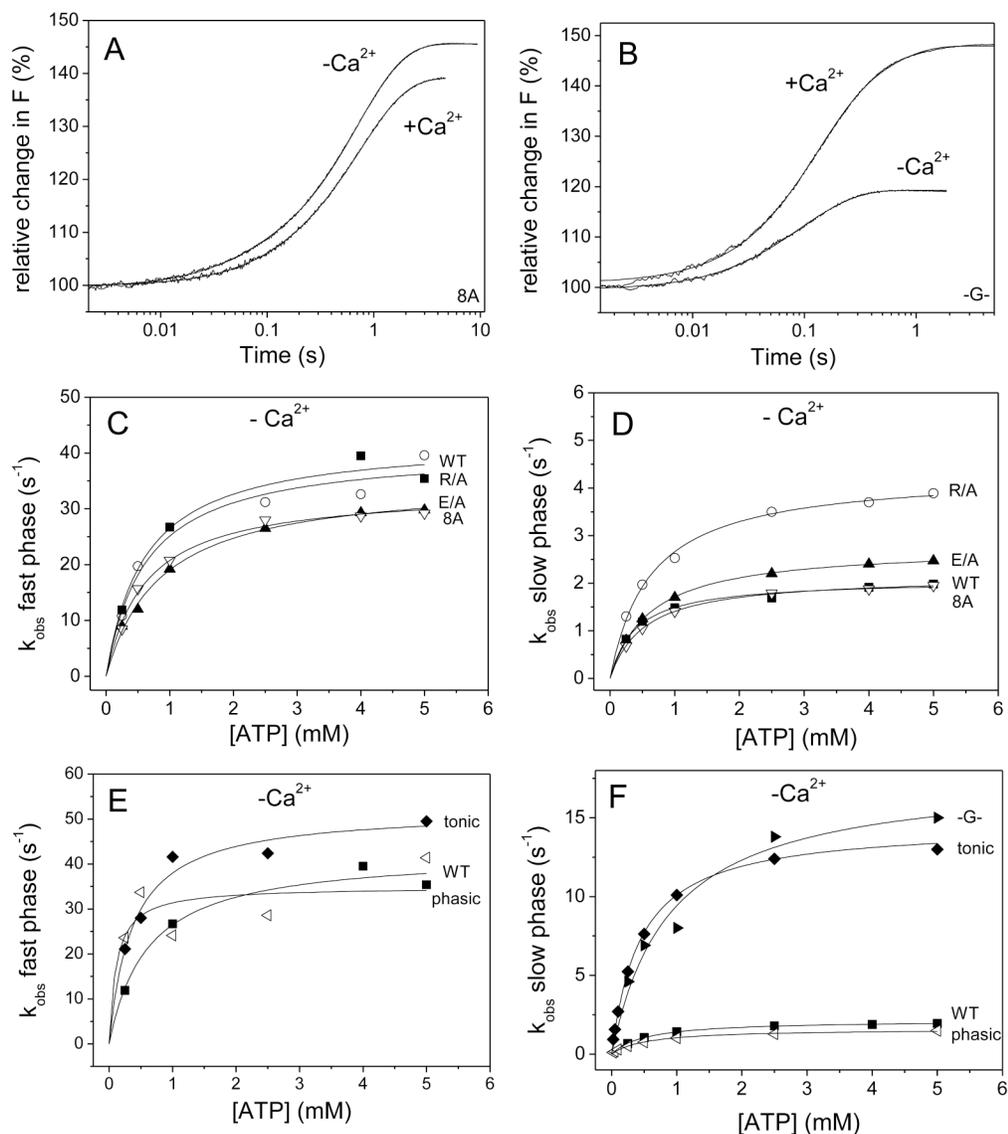
Figure 3.
ATP-induced dissociation of pyr.acto-Myo1c^{1IQ}. Pyrene fluorescence transients observed upon mixing 25 nM pyr.actin-Myo1c^{1IQ} chimeras with 1 mM ATP in the absence and presence of calcium. *A*, transients for Myo1c^{1IQ}-8A fitted to two exponentials (best fits superimposed): -Ca^{2+}: $k_{obs}1$ = 20.8 s^{-1}, A1 = 4.6 %, $k_{obs}2$ = 1.4 s^{-1}, A2 = 44.2 %; +Ca^{2+}: $k_{obs}1$ = 11.8 s^{-1}, A1 = 2.6 %, $k_{obs}2$ = 1.3 s^{-1}, A2 = 36.8 %. *B*, transients for pyr.actin-Myo1c^{1IQ}-G. The −Ca^{2+} transient was fitted to one exponential, the +Ca^{2+} transient to two exponentials (best fits superimposed): -Ca^{2+}: k_{obs} = 7.9 s^{-1}, A = 15.0 %; +Ca^{2+}: $k_{obs}1$ = 6.1 s^{-1}, A1 = 31.1 %, $k_{obs}2$ = 1.6 s^{-1}, A2 = 14.8 %. *C – F*, plots of the fast phase (*C & E*) and slow phase (*D & F*) k_{obs} for the chimeras as a function of [ATP] in the absence of calcium. Data were fitted to hyperbolae to obtain k_{max} and $K_{0.5}$ values: *C & D*, WT and alanine chimeras: *C*, fast phase k_{max} = 41±2 s^{-1} (WT ■), 41 ± 3 s^{-1} (R/A ○), 35 ± 1 s^{-1} (E/A ▲) and 34 ± 1 s^{-1} (8A ▽); $K_{0.5}$ = 507 ± 97 μM (WT), 622 ± 182 μM (R/A), 854 ± 75 μM (E/A) and 644 ± 57 μM (8A). *D*, slow phase: k_{max} = 2.0 s^{-1} (WT ■), 4.3 s^{-1} (R/A ○), 2.8 s^{-1} (E/A ▲) and 2.0 s^{-1} (8A ▽); $K_{0.5}$ = 370 ± 33 μM (WT), 623 ± 47 μM (R/A), 626 ± 11 μM (E/A) and 506 ± 18 μM (8A). *E & F*, smooth muscle loop and G chimeras: *E*, fast phase : k_{max} = 41 ± 2 s^{-1} (WT ■), 51 ± 2 s^{-1} (tonic ◆),

~49 ± 7 s^{-1} (phasic ◁); $K_{0.5}$ = 507 ± 97 μM (WT), 445 ± 49 μM (tonic), 1342 ± 479 μM (phasic). *F*, slow phase: k_{max} = 2.0 s^{-1} (WT ■), 14.6 s^{-1} (tonic ◆), 1.5 s^{-1} (phasic ◁) and 17.8 s^{-1} (G ▶); $K_{0.5}$ = 370 ± 33 μM (WT), 447 ± 13 μM (tonic), 468 ± 34 μM (phasic) and 888 ± 230 μM (G).
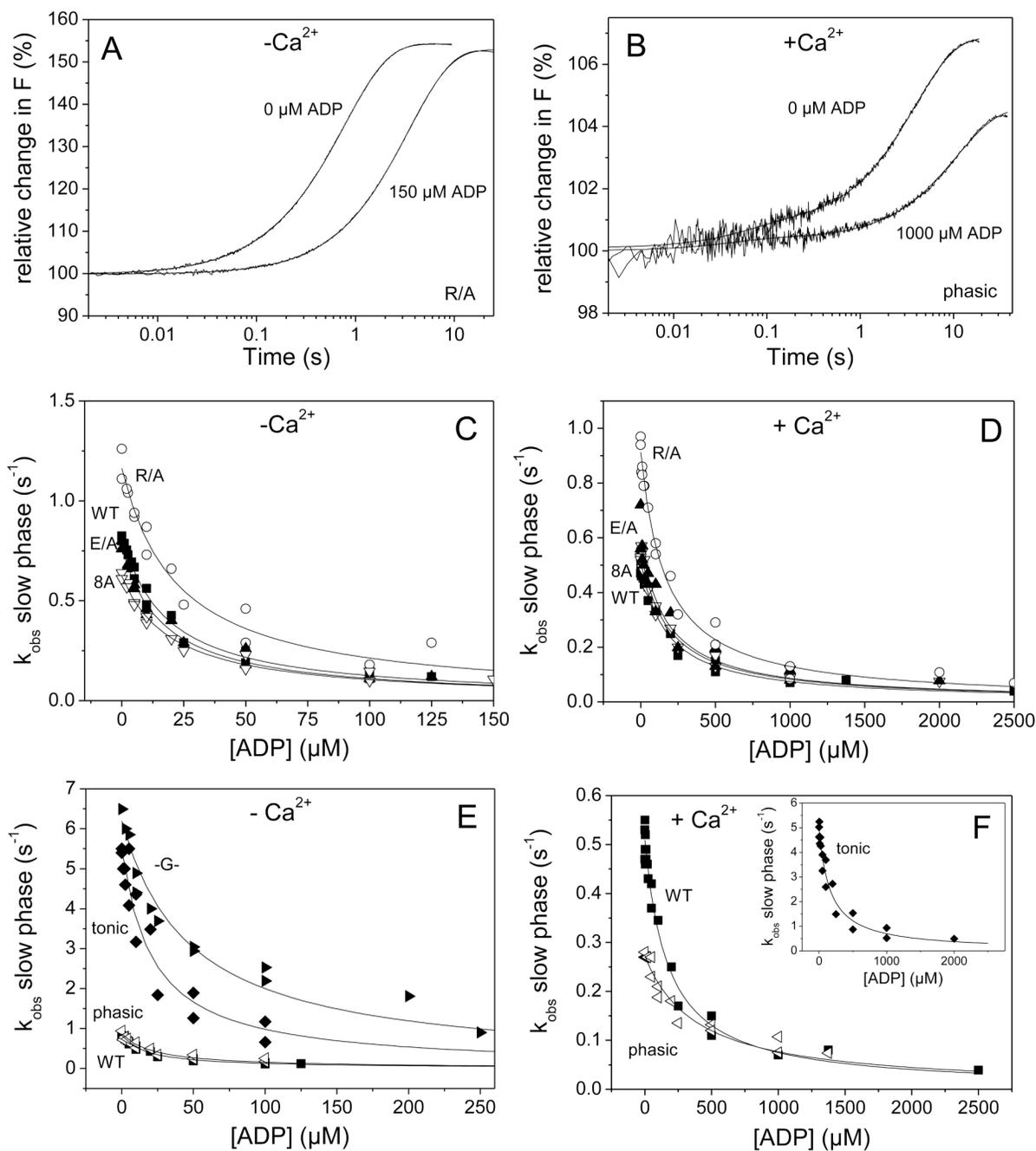
Figure 4.
Effect of ADP on ATP-induced dissociation of pyr.acto-Myo1c^{1IQ}. (A & B), pyrene
fluorescence transients of 25 nM pyr-acto-Myo1c^{1IQ} mixed with 250 μM ATP in the stopped-
flow apparatus in the absence or presence of high ADP for Myo1c^{1IQ}-R/A (-Ca^{2+}) and
Myo1c^{1IQ}-phasic (+Ca^{2+}). Transients in the absence of ADP were fitted to 2 exponentials,
transients in the presence of ADP were fitted to a single exponential: *A*, R/A: -ADP: $k_{obs}1 =$
11.0 s^{-1}, A1 = 3.0 %, $k_{obs}2 = 1.3$ s^{-1} A2 = 51.3 %; +ADP: $k_{obs} = 0.3$ s^{-1}, A = 52.8 %. *B*, phasic:
-ADP: $k_{obs}1 = 16.6$ s^{-1}, A1 = 0.8 %, $k_{obs}2 = 0.3$ s^{-1}, A2 = 6.0 %; +ADP: $k_{obs} = 0.9$ s^{-1}, A = 6.4
%. *C to F*, Increasing concentrations of ADP were either incubated with pyr.acto-Myo1c^{1IQ}
or ATP and the transients were fitted to two exponentials. The k_{obs} of the slow phases of both

experimental approaches was plotted together and fitted to a hyperbola to determine K_{app} and k_0 (in the absence *(C & E)* and presence of calcium *(D &F)*. *C & D*, alanine chimeras: -Ca^{2+}: K_{app} = 16.7 ± 1.9 µM (WT ■), 22.5 ± 2.9 µM (R/A ○), 17.0 ± 1.7 µM (E/A ▲), 20.3 ± 1.9 µM (8A ▽); k_0 = 0.82 s^{-1} (WT), 1.16 s^{-1} (R/A), 0.76 s^{-1} (E/A), 0.62 s^{-1} (8A); +Ca^{2+}: K_{app} = 173.6 ± 17.0 µM (WT), 166.1 ± 12.6 µM (R/A), 172.6 ± 30.3 µM (E/A), 180.0 ± 17.4 µM (8A); k_0 = 0.51 s^{-1} (WT), 0.91 s^{-1} (R/A), 0.59 s^{-1} (E/A), 0.55 s^{-1} (8A). *(E & F)*, smooth muscle myosin II loop 1 and G chimeras: -Ca^{2+}: K_{app} = 16.7 ± 1.9 µM (WT ■), 21.9 ± 4.2 µM (tonic ◆), 22.0 ± 3.5 µM (phasic ◁), 47.6 ± 6.3 µM (G▶); k_0 = 0.82 s^{-1} (WT), 5.5 s^{-1} (tonic), 0.87 s^{-1} (phasic), 6.2 s^{-1} (G); +Ca^{2+}: K_{app} = 173.6 ± 17.0 µM (WT), 165.2 ± 24.3 µM (tonic), 390.6 ± 46.1 µM (phasic); k_0 = 0.51 s^{-1} (WT), 4.92 s^{-1} (tonic), 0.27 s^{-1} (phasic), (no data for G).
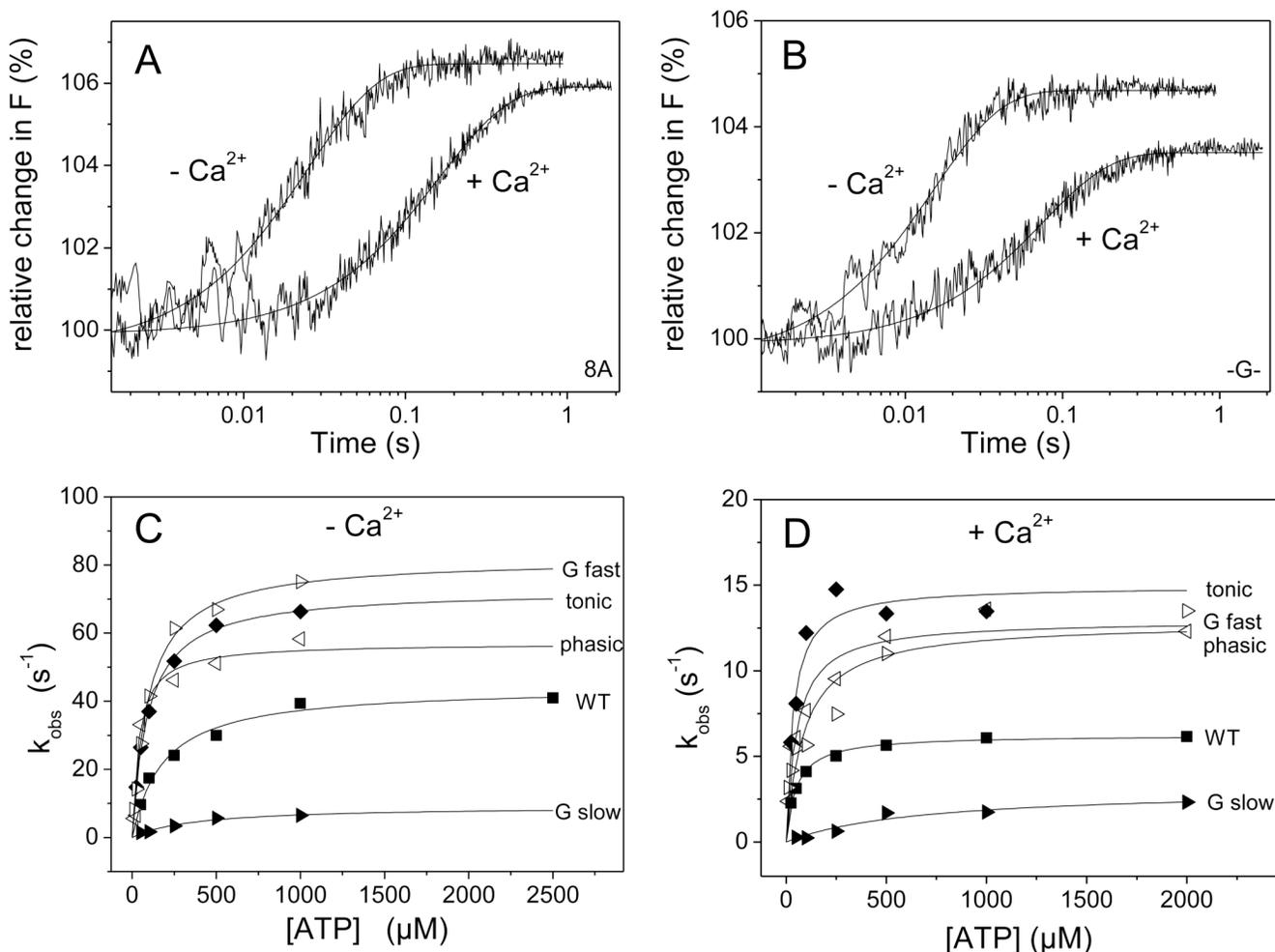
Figure 5.
ATP binding to Myo1c[1IQ] loop 1 chimera. *A & B*, Protein fluorescence transients observed upon mixing 50 nM Myo1c[1IQ] with 1 mM ATP in the absence and presence of calcium (concentrations after mixing). Data were fitted to a single exponential (best fit superimposed): *A*, Myo1c[1IQ]-R/A -Ca^{2+}: $k_{obs} = 41.6$ s^{-1}, A = 6.3 %; +Ca^{2+}: $k_{obs} = 5.7$ s^{-1}, A = 5.8 %. *B*, Myo1c[1IQ] –tonic: -Ca^{2+}: $k_{obs} = 66.3$ s^{-1}, A = 4.5 %; +Ca^{2+}: $k_{obs} = 13.5$ s^{-1}, A = 3.5 %. *C & D*, k_{obs} of each chimera plotted as a function of ATP concentration. Data were fitted to hyperbolae (best fits superimposed): *C*, fitted values in the absence of calcium $k_{max} = 44.3 \pm 1.9$ s^{-1} (WT ■), 72.8 ± 1.1 s^{-1} (tonic ◆), 61.1 ± 10.3 s^{-1} (phasic ◁), 9.1 ± 0.2 s^{-1} (G slow ▶), 82.5 ± 1.9 s^{-1} (G fast ▷); $K_{0.5} = 184 \pm 22$ μM (WT), 94.5 ± 4.8 μM (tonic), 75 ± 30 μM (phasic), 100.0 ± 7.7 μM (G fast), 381 ± 102 μM (G slow). *D*, Fitted values in presence of calcium: $k_{max} = 6.3 \pm 0.1$ s^{-1} (WT), 15.0 ± 0.9 s^{-1} (tonic), 13.0 ± 0.7 s^{-1} (phasic), ~3 s^{-1} (G slow), 13.1 ± 1.4 s^{-1} (G fast); and $K_{0.5} = 49.5 \pm 3.4$ μM (WT), 34.4 ± 9.9 μM (tonic), 52.0 ± 11.9 μM (phasic), 100.3 ± 38.3 μM (G fast), 670 ± 295 μM (G slow).
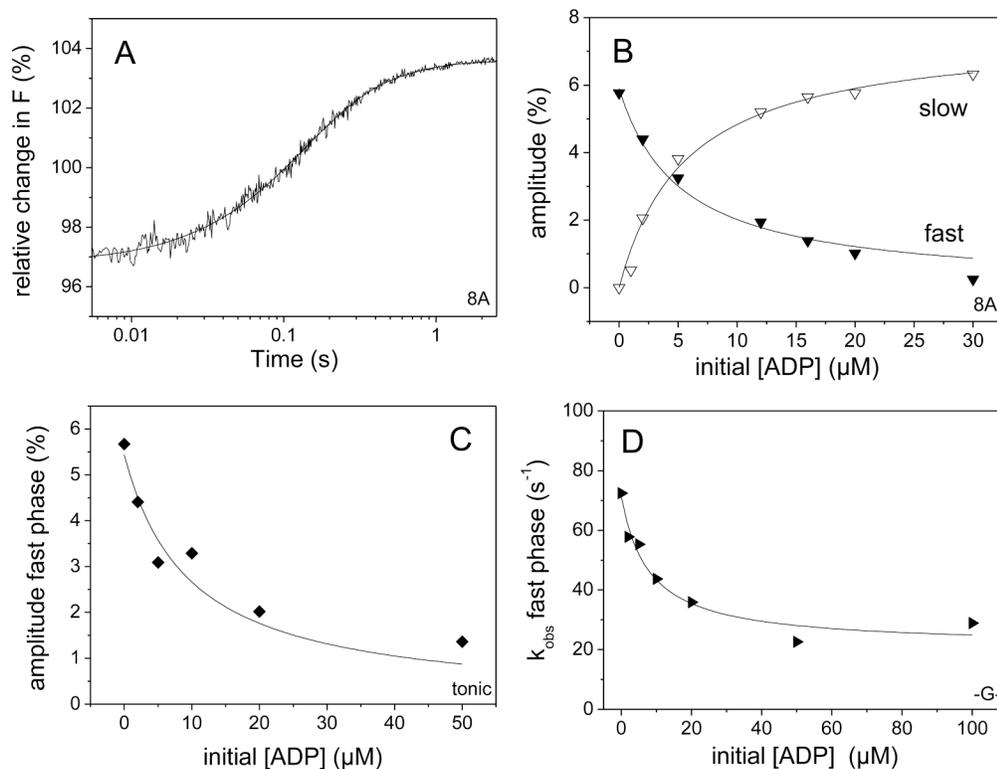
Figure 6.
ADP displacement from Myo1c^{1IQ} loop 1 chimeras in the absence of calcium. *A*, Protein fluorescence transient observed upon displacing 10 μM ADP from 50 nM Myo1c^{1IQ}-8A by addition of 0.5 mM ATP. The change in fluorescence was fitted to two exponentials: $k_{obs}1 = 8.1$ s^{-1}, $k_{obs}2 = 2.3$ s^{-1}, A1 = 1.7 %, A2 = 5.1 %. *B*, Plot of the fast and slow amplitudes of the ADP displacement experiment for Myo1c^{1IQ}-8A as a function of [ADP]. The data were fitted to a hyperbola to obtain the K_D. K_D, fast = 5.2 ± 0.8 μM, K_D, slow = 5.7 ± 1.1 μM. *C*, plot of the fast phase amplitude of the ADP-displacement experiment with Myo1c^{1IQ}-tonic as a function of [ADP]. A fit to a hyperbola defined $K_D = 9.2 ± 1.6$ μM. *D*, plot of the fast phase k_{obs} of the ADP displacement experiment with Myo1c^{1IQ}-G as a function of [ADP]. A fit to a hyperbola defined $K_D = 7.9 ± 3.0$ μM with $k_0 = 71$ s^{-1}.
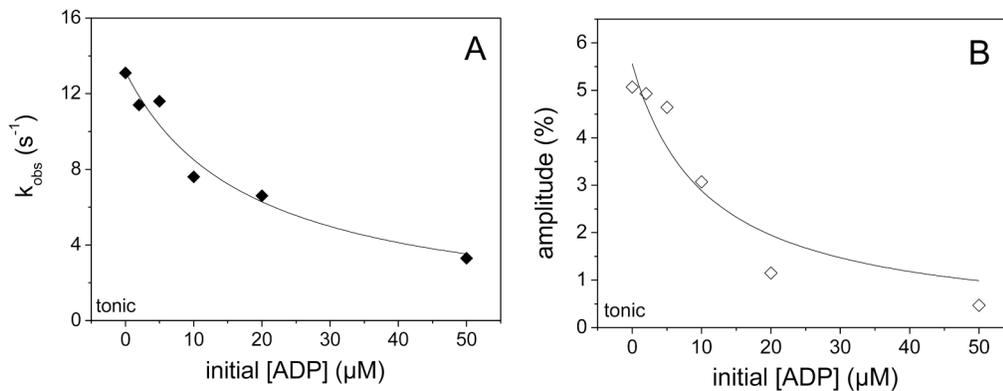
Figure 7.
ADP displacement from Myo1c[1IQ]-tonic in the presence of calcium. 50 nM Myo1c[1IQ]-tonic was incubated with increasing concentrations of ADP and then mixed with 0.5 mM ATP in the stopped-flow system and the change in protein fluorescence monitored over time. *A*, plot of the k_{obs} as a function of [ADP]. The data of the fast phase were fitted to a hyperbola to determine the $K_D = 18.2 \pm 3.7$ μM with $k_0 = 13.1$ s^{-1}. *B*, plot of the amplitude as a function of [ADP]. A fit to a hyperbola determined the $K_D = 10.8 \pm 4.2$ μM.
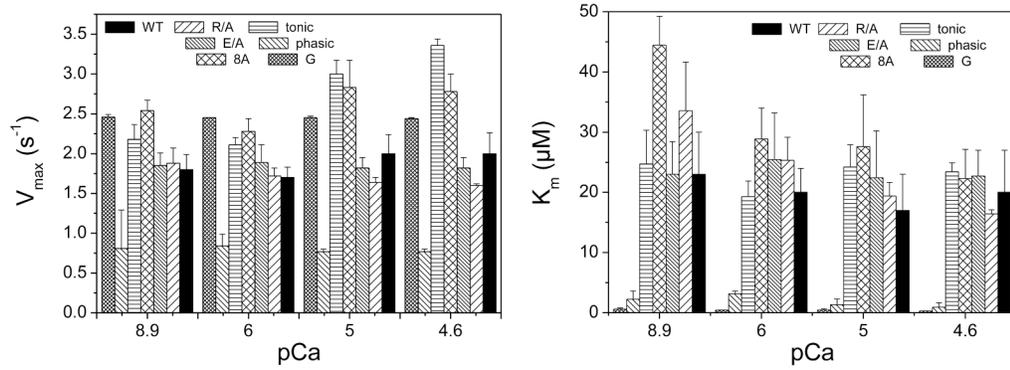
Figure 8.
Steady-state actin-activated ATPase activity of Myo1c^{1IQ} and loop 1 mutants. Plotted are the values of V$_{max}$ (left) and K$_m$ (right) at pCa 4, 5, 6 and 8.9 for Myo1c^{1IQ}-WT and each of the loop 1 mutants used in the study.

$$\text{A·M'} \underset{k_{-\alpha}}{\overset{k_{+\alpha}}{\rightleftharpoons}} \text{A·M + T} \underset{}{\overset{K_1}{\rightleftharpoons}} \text{A·M·T} \underset{}{\overset{k_{+2}}{\rightleftharpoons}} \text{A~M·T} \xrightarrow{k_{dissn}} \text{A + M·T} \underset{k_{-3}}{\overset{k_{+3}}{\rightleftharpoons}} \text{A + M·D·P}_i$$

K_α

CLOSED   OPEN   OPEN

A·M·D

k_{-AD} D

K_{AD}

D

k_{+AD}

Scheme 1.

$$M + T \underset{k_{-1}}{\overset{k_{+1}}{\rightleftharpoons}} M{\cdot}T \underset{k_{-2}}{\overset{k_{+2}}{\rightleftharpoons}} M^*T \underset{k_{-3}}{\overset{k_{+3}}{\rightleftharpoons}} M^{**}D{\cdot}P_i \underset{k_{-4}}{\overset{k_{+4}}{\rightleftharpoons}} M^*D{\cdot}P_i \underset{k_{-5}}{\overset{k_{+5}}{\rightleftharpoons}} M^*D+P_i \underset{k_{-6}}{\overset{k_{+6}}{\rightleftharpoons}} M{\cdot}D \underset{k_{-7}}{\overset{k_{+7}}{\rightleftharpoons}} M+D$$
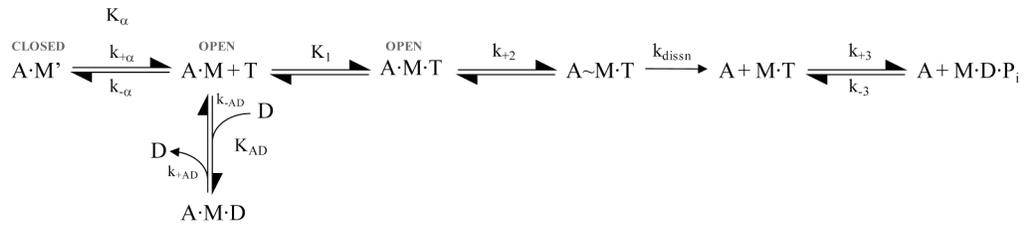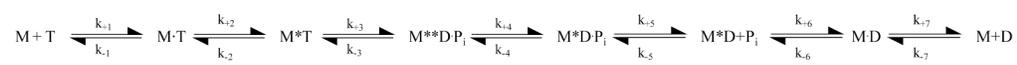
Scheme 2.

Table 1

Values for k_{+2}, $k_{+\alpha}$ and K_α for the acto-Myo1c^{1IQ} loop 1 chimeras in the absence and presence of calcium

	$k_{+\alpha}(s^{-1})$		k_{+2} (s^{-1})		K_α	
	-Ca^{2+}	+Ca^{2+}	-Ca^{2+}	+Ca^{2+}	-Ca^{2+}	+Ca^{2+}
WT	2.0	2.7	41 ± 2	20 ± 4	0.12	0.11
R/A	4.3	4.6	41 ± 3	110 ± 34	0.11	0.08
E/A	2.8	3.1	35 ± 1	55 ± 18	0.12	0.05
8A	2.0	2.8	34 ± 1	22 ± 5	0.10	0.08
tonic	14.6	14.5	51 ± 2	95 ± 8	0.21	0.12
phasic	1.5	1.0	49 ± 7	-	0.09	0.23
G	17.8	5.7	17.8	18.4	#nd	1.8

#not defined

Table 2

ADP affinities (K_D) and ADP release rate constants (k_{-D}) measured for the loop 1 chimeras in the presence and absence of actin and calcium

	K_D (μM)		k_{+D} (s⁻¹)		K_{AD} (μM)		k_{+AD} (s⁻¹) (calculated)	
	$-Ca^{2+}$	$+Ca^{2+}$	$-Ca^{2+}$	$+Ca^{2+}$	$-Ca^{2+}$	$+Ca^{2+}$	$-Ca^{2+}$	$+Ca^{2+}$
WT	3.3 ± 1.5	Nd[#]	6	4	1.74	16.9	2.1	20.3
R/A	6.4 ± 1.7	Nd[#]	7	4[*]	2.22	12.6	2.4	13.9
E/A	4.4 ± 1.0	Nd[#]	5	4[*]	1.82	8.6	2.7	12.9
8A	5.5 ± 1.0	Nd[#]	5	4[*]	1.85	13.2	4.4	31.7
tonic	9.2 ± 1.6	~11	7	>15	3.80	17.7	4.9	23.0
phasic	Nd	Nd	37	Nd	1.83	73.1	~2	~73
G	15.1 ± 8.5	-	25-30	Nd	4.32	-	~4	-

[*]
assumed to be similar to WT with no change in calcium

[#]
assumed to be similar to $-Ca^{2+}$ as for WT

Nd, not determined

Table 3

ATP binding to Myo1c^{1IQ} loop 1 chimeras in the absence and presence of calcium

| | k_{max} (s^{-1}) = k_{+3}+k_{-3} | | | $K_{0.5}$ (µM) (=1/K_1) | | |
	-Ca^{2+}	+Ca^{2+}	Ratio -/+Ca^{2+}	-Ca^{2+}	+Ca^{2+}	Ratio -/+Ca^{2}
WT	44.3 ± 1.9	6.3 ± 0.1	7.0	184 ± 22	49.5 ± 3.4	3.7
R/A	45.5 ± 1.9	5.9 ± 0.3	7.7	153 ± 24	54.0 ± 12.2	2.8
E/A	49.6 ± 1.1	7.9 ± 0.2	6.3	255 ± 14	65.6 ± 7.5	3.9
8A	37.2 ± 0.5	5.9 ± 0.3	6.3	179 ± 8	62.2 ± 12.0	2.9
tonic	72.8 ± 1.1	15.0 ± 0.9	4.9	95 ± 5	34.4 ± 9.9	2.8
phasic	61.1 ± 10.3 *	13.0 ± 0.7	4.7	75 ± 30	52.0 ± 11.9	1.4
G	82.5 ± 1.9	13.1 ± 1.4	6.3	100 ± 8	100.3 ± 38.3	1
G$_{slow}$	9.1	~3	3	381 ± 102	670 ± 295	0.5

* larger error due to smaller amplitude

Table 4

Myo1c^{SAH}-mediated movement of actin filaments in vitro*

Construct	movement of actin in nm/s
Myo1c^{SAH}-WT	12 ± 4 (353)
Myo1c^{SAH}-tonic	22 ± 7 (587)
Myo1c^{SAH}-phasic	5 ± 3 (318)
Myo1c^{SAH}-G	29 ± 7 (455)

*
Data are presented as average speed ± standard deviation (number of filaments analyzed)